Near-field optical model for directed energy-propelled spacecrafts

Amber Sucich, Tomas Snyder, Gary B. Hughes, Prashant Srinivasan, Philip Lubin, et al.

Amber Sucich, Tomas Snyder, Gary B. Hughes, Prashant Srinivasan, Philip Lubin, Qicheng Zhang, Alexander Cohen, Jonathan Madajian, Travis Brashears, Nic Rupert, "Near-field optical model for directed energy-propelled spacecrafts," Proc. SPIE 10401, Astronomical Optics: Design, Manufacture, and Test of Space and Ground Systems, 1040107 (5 September 2017); doi: 10.1117/12.2274692

SPIE.

Event: SPIE Optical Engineering + Applications, 2017, San Diego, California, United States

Near field optical model for directed energy propelled spacecraft

Amber Sucich[a], Tomas Snyder[a], Gary B. Hughes[b], Prashant Srinivasan[a], Philip Lubin[c], Qicheng Zhang[c], Alexander Cohen[c], Jonathan Madajian[c], Travis Brashears[c], and Nic Rupert[c]
gbhughes@calpoly.edu
lubin@deepspace.ucsb.edu
[a]Physics Department, California Polytechnic State University, San Luis Obispo, CA 93407-0405
[b]Statistics Department, California Polytechnic State University, San Luis Obispo, CA 93407-0405
[c]Physics Department, University of California, Santa Barbara, CA 93106-9530

ABSTRACT

Directed energy is envisioned to drive wafer-scale spacecraft to relativistic speeds. Spacecraft propulsion is provided by a large array of lasers, either in Earth orbit or stationed on the ground. The directed-energy beam is focused on the spacecraft sail, and momentum from photons in the laser beam is transferred to the spacecraft as the beam reflects off of the sail. In order for the beam to be concentrated on the spacecraft, precise phase control of all the elements across the laser array will be required. Any phase misalignments within the array will give rise to pointing fluctuations and flux asymmetry in the beam, necessitating creative approaches to spacecraft stability and beam following. In order to simulate spacecraft acceleration using an array of phase-locked lasers, a near field intensity model of the laser array is required. This paper describes a light propagation model that can be used to calculate intensity patterns for the near-field diffraction of a phased array. The model is based on the combination of complex frequencies from an array of emitters as the beams from each emitter strike a target surface. Ray-tracing geometry is used to determine the distance from each point on an emitter optical surface to each point on the target surface, and the distance is used to determine the phase contribution. Simulations are presented that explore the effects of fixed and time-varying phase mis-alignments on beam pointing, beam intensity and focusing characteristics.

Keywords: Directed Energy, Laser Propulsion, Interstellar Travel

1. INTRODUCTION

1.1. Background

For many years, directed energy has been envisioned as a source of photon pressure that could be used to accelerate small spacecraft to relativistic speeds.[1-14] In a modern vision, the entire spacecraft is a gram-scale device that would include all mission components imbedded in a semiconductor wafer, including power, laser communications, photon-thruster or micro-reaction wheel attitude control, imaging and other sensors.[15-18] For propulsion, the driving force is provided by radiation pressure from a large array of phase-locked lasers, either in Earth orbit or stationed on the ground.[12-15] Fig. 1 is an artist's conception of a ground-based laser array that would propel a small spacecraft which could be pre-positioned in Earth orbit by being jettisoned from an orbiting platform. The directed-energy beam from the ground-based array is focused on the spacecraft's sail, propelling it out of Earth orbit on a path to its ultimate destination. The acceleration phase would be short, while the spacecraft is within focusing range of the laser array. Once the craft is beyond the useful range of the laser, no additional acceleration occurs.

One critical issue with laser propulsion using a large laser array is beam formation: pointing jitter and intensity fluctuations within the beam will result in asymmetric flux on the spacecraft sail.[18-21] In order to utilize radiation pressure from the laser beam, the spacecraft sail design must include passive righting mechanisms that compensate for asymmetric flux, maintaining the sail orientation approximately normal to the directed-energy beam during the acceleration phase. Furthermore, to ensure that the spacecraft moves laterally to follow the beam as pointing jitter occurs, some combination of sail design and beam shaping will be required. Development of yaw stability and beam following designs will require realistic models of laser beam intensity impinging on the spacecraft sail. This paper describes a near-field model of light intensity produced by an array of lasers where the phase of individual emitters is controllable. The model is based on geometrical ray-tracing: the light path from each point on the surface of an emitter optical element to any location on a selected target surface is determined. The complex phases from each emitter are summed to determine the beam intensity at each point on the target surface.

Astronomical Optics: Design, Manufacture, and Test of Space and Ground Systems, edited by Tony B. Hull, Dae Wook Kim, Pascal Hallibert, Gary B. Hughes, Ronald G. Pirich, Proc. of SPIE Vol. 10401, 1040107 · © 2017 SPIE · CCC code: 0277-786X/17/$18 · doi: 10.1117/12.2274692

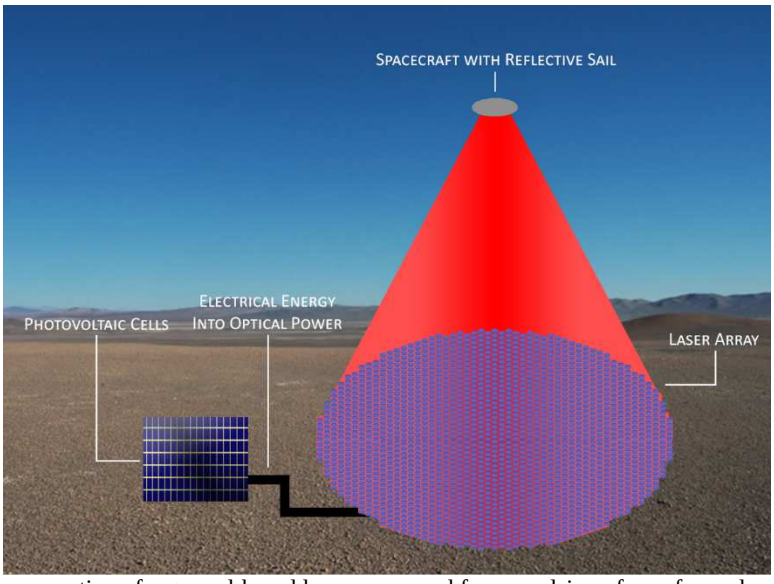

Figure 1. Artist's conception of a ground-based laser array used for propulsion of a wafer-scale spacecraft. The phases of individual emitters are controlled, so that constructive interference at the target maximizes beam intensity on the spacecraft sail. Phase misalignments within the array lead to pointing jitter and asymmetry in the beam, creating challenges for spacecraft stability.

1.2. Prior Art

A far-field model for beam intensity produced by a coherently-combined laser array was described in previous work, based on combining complex phases from each source based on the angle between the array normal and a target direction vector.[22] The far-field model makes several simplifying assumptions about geometry, in particular that the target is distant enough so that the angle between the target and each emitter is constant. The conventional configuration is displayed in Fig. 2, is identical to a diffraction grating model.

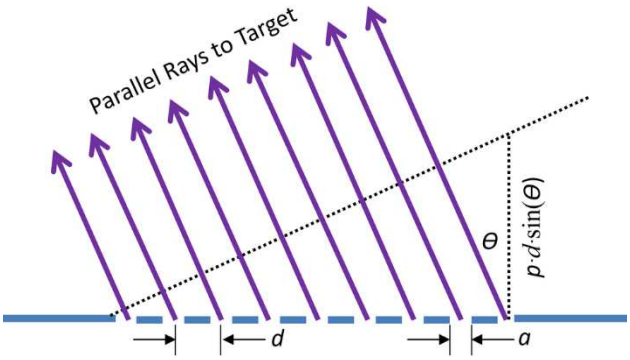

Figure 2. Classical depiction of a diffraction grating. The aperture of each slit is designated by *a*, and the slit pitch is *d*, e.g. both in meters. Determination of light intensity at a 'distant' target assumes that the angle between the target and every slit is the same. Combining complex phases from each emitter at the target is accomplished with the resulting geometry, based on the phase from each emitter at the target plane.

Based on the geometry and assumptions that are inherent in Fig. 2, the complex far-field amplitude for a linear array of N emitters with wavelength λ, pitch d, aperture a, and including static (E_f) and time-varying (E_t) phase misalignments at each emitter is found by summing the complex phases from each emitter:[22]

$$U(\theta,t) = \frac{e^{[i\cdot k\cdot a\cdot sin(\theta)]} - 1}{i\cdot k\cdot sin(\theta)} \cdot \sum_{p=0}^{N-1} e^{\{i\cdot[k\cdot p\cdot d\cdot sin(\theta)+E_s(p)+E_t(p,t)]\}} \quad (1)$$

Terms are defined in Table 1. The model is suitable for estimating far-field beam intensity, under some assumptions about the source of phase misalignment in a coherently-combined laser array. The model includes static phase mis-alignments at each emitter, such as might arise from component mounting errors. The model also includes time-varying phase mis-alignments at each emitter, which could be created by mechanical vibration, thermal fluctuations, phase noise in the seed laser and transmission fibers, etc.

1.3. A Baseline Mission Scenario

The far-field model assumes that the direction from each emitter to the target is the same. However, this classical assumption is not met in a scenario where an Earth-based laser array is focusing on a wafer-scale spacecraft that begins the acceleration phase in Earth orbit. Consider a ground-based array, such as depicted in Fig. 1. Further consider that a wafer-scale spacecraft with a reflective sail will be deployed to a launch position in Earth orbit. That is, a wafer-scale interstellar probe is envisioned to be ejected from a larger vessel that is in Earth orbit. Once the wafer-scale craft is ejected, the laser array is activated to accelerate the craft into its mission trajectory. The larger vessel is envisioned to contain many wafer-scale spacecraft that could be launched in succession. In this scenario, the distances involved are incompatible with the far-field assumption depicted in Fig. 2, since the initial distance between the laser array and the spacecraft is small enough to create significantly different angles between the spacecraft and individual array elements.

Consider, for purposes of illustration, a wafer-scale spacecraft with a 1 m diameter sail. Suppose that the goal for a single laser emitter is to fill the sail when the craft is 10 km away. This distance is chosen to accentuate the difference between near-field and far-field models, but the same effects will be present at greater distances. To precisely fill the 1 m diameter sail when the craft is 10 km away, the angular field of view (FOV) of the emitter should be 10^{-4} rad. Suppose that the laser emitters are in a planar array on the ground, and that the optical axis of each emitter is adjustable. Suppose the optical axis of one emitter is orthogonal to the emitter plane, and directed at the center of the sail. Then, adjacent emitters that are also orthogonal to the emitter plane will not be directing their beam profiles onto the sail. The optical axes of every emitter must be adjusted toward the desired center of the beam pattern on the target surface, depicted in Fig. 3.

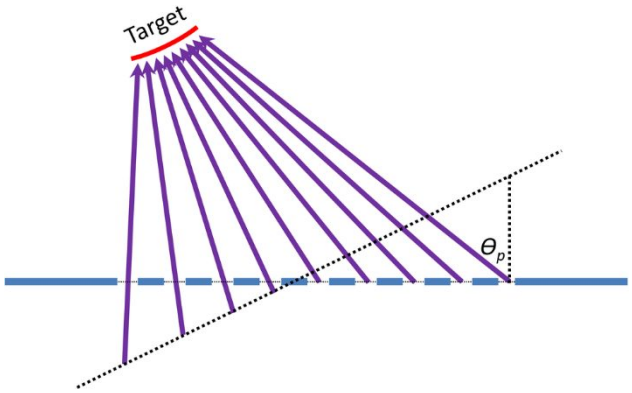

Figure 3. The optical model for beam intensity must accommodate different angles from each emitter to the target. This condition is incompatible with the far-field model depicted in Fig. 2.

1.4. Optical Models for Design Development

For a mission that seeks a 1 m beam on a target that is 10 km distant, individual emitters will be coupled to lens elements that are ~0.5 m in diameter. The overall laser array will be made up of many individual emitters, e.g., let *N* denote the total number of emitters in the array. For deep-space missions, the area spanned by *N* emitters will be several square kilometers. In order to model the beam intensity at the target, it is clear that the far-field assumption is inadequate, since the total aperture of the system is large and the distance to the target is, at least initially, short. A revised optical model is required that accounts for different angles between each emitter and the target, as depicted in Fig. 4. The model must account for the 3-dimensional position of each emitter with respect to the target, as well as changes in the positions of all components through time. The model must also account for the current optical axis of each emitter, including changes in the optical axis through time.

2. A NEAR-FIELD BEAM MODEL

2.1. Near-Field Model Description

The model is based on the sum of complex phases from each source, accounting for the three-dimensional distance between each point on a lens element to a selected point on the target surface. In the model, an array of N emitters is represented by prescribing the (nominal) location of each individual emitter, and associated lens diameter and optical axis pointing vectors. To begin, the emitter pattern is established as a circular close-packed array, according to the diameter of a single lens element (lenses are all the same size, for simplicity). Each of the N lenses is then 'discretized' into n_{pts} individual locations that are also arranged in a circular-close-packed pattern within the lens element, depicted in Fig. 2. The intensity at any location $\langle x, y, z\rangle$ in front of the lens is calculated by summing complex phases from contributions of discretized points on each lens. For the scenario of a laser-propelled spacecraft, the near field intensity is calculated on some target surface. For example, the target surface could be the sail surface area. The general scheme for determining near-field beam intensity is expressed in Eq. (2), with terms defined in Table 1.

$$U(\langle x.y,z\rangle,t)=\sum_{p=0}^{N-1}\left[\sum_{s_p=1}^{n_{pts}}\left(\frac{e^{\left[i\cdot k\cdot a\cdot sin\left(\theta_{s_p}\right)\right]}-1}{i\cdot k\cdot sin\left(\theta_{s_p}\right)}e^{\{i\cdot k\cdot[\varphi'(s_p)+E_s(s_p)+E_t(s_p,t)]\}}\right)\right] \tag{2}$$

Given the complex amplitude, the near-field beam intensity at a point on the target surface is then:

$$I(\langle x,y,z\rangle,t)=|U(\langle x,y,z\rangle,t)|^2 \tag{3}$$

Table 1. Definition of terms used for model simulations presented in this paper.

Symbol	Interpretation	Units
U	Complex amplitude as a combination of contributions from N emitters at a point $\langle x, y, z\rangle$ on the target at time t	complex
N	Number of emitters in the laser array	count
n_{pts}	Number of discretization points in each lens	count
λ	Nominal emitter wavelength (1.064 μm)	μm
k	$2\pi/\lambda$	rad μm^{-1}
$\varphi'(s_p)$	Phase Distance from a point s_p on the lens to a point $\langle x, y, z\rangle$ on the phase reference surface, modulo λ (Eq. (11))	μm
θ_{s_p}	Angle between the optical axis of a lens, and a vector from a point s_p on the lens to point $\langle x, y, z\rangle$ on the target	rad
a	Discretization radius	μm
$E_s(s_p)$	Static phase mis-alignments at each discretized emitter location s_p	rad
$E_t(s_p,t)$	Time-varying phase mis-alignments at each discretized emitter location s_p at time t	rad
I	Near-field beam intensity as a combination of contributions from N emitters at a point $\langle x, y, z\rangle$ on the target at time t	W/m^2

Implementation of the model depends on the geometry of the emitters with respect to the target surface. The emitter pattern is created according to the diameter of a lens element, and then each lens is 'discretized' into n_{pts} individual points (Fig. 2). The target surface is defined, and then discretized. At each discretized point on the target, the sum of complex amplitudes in Eq. (2) is calculated for contributions from all of the discretized points in the emitter plane. For the simulations described in this paper, the laser array is constructed from lens elements of a prescribed size. The first emitter is initially centered at the origin, and oriented within the x-y plane. Additional emitters are added to the array in hexagonal 'shells' around the periphery of any existing elements. The first shell will have six emitters, located

at the vertices of a hexagon that is centered at the origin. The k^{th} shell will have emitters at the vertices of a larger hexagon, and also k - 1 emitters along each edge of the hexagon.

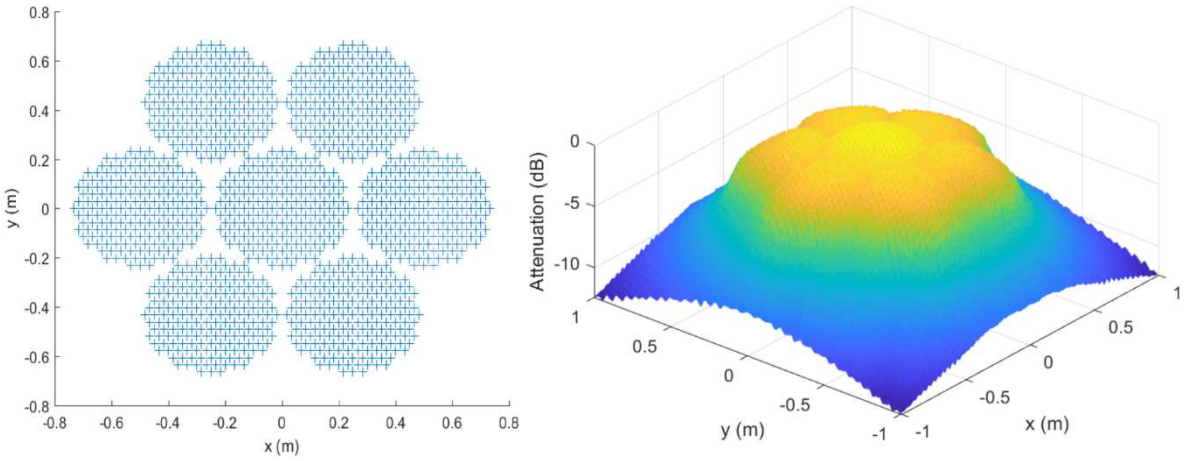

Figure 4. Left: A 7-element array is depicted, with each lens being discretized. **Right**: The beam intensity on a selected target surface is modeled as the combination of complex amplitudes from each emitter. For the 7-element array shown, and with the optical axis of each emitter orthogonal to the target plane, the modeled beam intensity on an orthogonal target plane 10000 m from the source is shown.

To create the discretization pattern for each lens, a nominal pattern is created in the *x*-*y* plane, and centered at the origin. The discretization points are created in shells in a manner similar to the pattern of emitters in the overall array. Once the nominal pattern is created, the discretization points are then rotated to the optical axis direction, and translated out to the nominal position of the associated emitter. The repositioning is accomplished by first applying a general rotation around the origin through an angle determined by the prescribed optical axis pointing vector. The rotation axis $N = \langle N_x, N_y, N_z \rangle$ is the cross product of the optical axis pointing vector and a vector from the center of the array to the center of the target, and the rotation angle Θ is the angle between the two vectors. The rotation about the origin is accomplished by applying a rotation matrix:

$$\begin{bmatrix} \cos(\theta) + N_x^2[1-\cos(2\theta)] & -N_z\sin(\theta) + N_xN_y[1-\cos(\theta)] & N_y\sin(\theta) + N_y\,N_z[1-\cos(\theta)] \\ N_y\sin(\theta) + N_xN_y[1-\cos(2\theta)] & \cos(\theta) + N_y^2[1-\cos(\theta)] & -N_x\sin + N_yN_z[1-\cos(\theta)] \\ -N_y\sin(\theta) + N_xN_y[1-\cos(2\theta)] & N_x\sin(\theta) + N_yN_z[1-\cos(\theta)] & \cos(\theta) + N_z^2[1-\cos(\theta)] \end{bmatrix} \quad (4)$$

The rotated points are then translated out to put the center of the pattern at the nominal (prescribed) location of the emitter within the array. The process is repeated for each lens element in the laser array.

The model implementation is based on the concept of a phase reference surface, a virtual surface that provides a datum for alignment of phases from each emitter. The phase reference surface is a projection of the target, placed between the target and the emitter array. That is, the normal distance from the target surface to the reference surface is constant. The model assumes that no phase perturbation arises between the phase reference surface and the target, i.e., that the coherence length of the laser system is longer than the path length to the target. So, the phase alignment at the reference surface is the same as the phase alignment at the target surface. For simplicity, consider the target surface to be a plane (although any surface can be modeled). Then, the phase reference surface is also a plane which is normal to the target plane normal vector. For convenience, the phase reference plane can be anchored to the center of the array, but the anchor point is arbitrary. Distances from a point on the reference plane to the emitter surface are found using ray-tracing geometry. Suppose a point $P = \langle P_x, P_y, P_z \rangle$ lies at some location on an emitter. The complex phase contributed to a point $Q = \langle Q_x, Q_y, Q_z \rangle$ in the target plane is to be calculated. The unit-length direction vector from P to Q is

$$E = \frac{\langle Q_x - P_x, Q_y - P_y, Q_z - P_z \rangle}{\left\| \langle Q_x - P_x, Q_y - P_y, Q_z - P_z \rangle \right\|} \quad (5)$$

The ray from P_i to Q_i will trace a path along the direction vector E_i from point Q_i to a point R_i on the phase reference plane, over some path distance t_i:

$$R_i = P_i + t_i \cdot E_i \tag{6}$$

The distance t_i can be determined directly, since P_i lies in the emitter plane, and the reference plane is defined in space by the anchor point and the target normal vector.[23] For a reference plane anchor point A, and a unit-length target normal vector V, the reference plane equation is:

$$V \cdot \langle x, y. z \rangle = V \cdot A \tag{7}$$

Since the point R_i lies in the reference plane, it satisfies the plane equation, so substitute the expression for R_i from Eq. (6) into Eq. (7):

$$V \cdot (P_i + t_i \cdot E_i) = V \cdot A \tag{8}$$

Distribute the inner product across the sum in Eq. (8) to solve for the distance t_i:

$$t_i = \frac{V \cdot (A - P_i)}{V \cdot E_i} \tag{9}$$

Where V is the reference plane normal vector, A is the reference plane anchor (arbitrary, but fixed), and E_i is the unit-length direction vector from P_i on the emitter plane to Q_i on the target plane. The points R_i are then found by:

$$R_i = P_i + \left(\frac{V \cdot (A - P_i)}{V \cdot E_i} \right) \cdot E_i \tag{10}$$

The central idea of the model is that the phase alignment across the points R_i will be the same as the phase alignment of the corresponding rays in the target plane. The model assumes that the phase of each emitter is controllable, so the exit phases at the emitter points P_i are all known. The phases at the points R_i on the reference plane can be calculated from the exit phases at P_i and the associated distances, t_i, by adding the phase difference t_i modulo λ to the emitter exit phase:

$$\varphi_i' = \varphi_i + (t_i \text{ modulo } \lambda) \tag{11}$$

The resulting phase difference determines the complex phase at the corresponding point on the target, used in Eq. (2). Phase perturbations (fixed and/or time-varying) can be added to the phase from each emitter point, by adding an error term to the phase distance calculated by Eq. (11). Depending on the location of the reference plane, the distances t_i may be large in comparison to the wavelength, raising the possibility that round-off error could affect the calculations. Modular multiplication and exponentiation rules can be exploited to simplify the calculation, namely:

$$A \cdot B^k \bmod C = \{(A \bmod C) \cdot [(B \bmod C)^k \bmod C]\} \bmod C \tag{12}$$

The general rule can be further adapted for the current scenario. For λ = 1.064e-6 m, round to a fixed-precision integer, and move the exponent to the left hand side:

$$A \cdot 10^{k+9} \bmod 1064 = \{(A \bmod 1064) \cdot [(10 \bmod 1064)^{k+9} \bmod 1064]\} \bmod 1064 \tag{13}$$

Here, A is in the interval [1, 10), so A mod 1064 = A. Likewise, 10 mod 1064 = 10. The expression simplifies to a form that is less susceptible to round-off error:

$$\varphi_i' = \text{sign}(t_i) \cdot (\{A \cdot [10^{k+9} \bmod 1064]\} \bmod 1064) \cdot 10^{-9} \tag{14}$$

Where:

$$k = \text{floor}\{\log_{10}[\text{abs}(t_i)]\} \tag{15}$$

$$A = \frac{\text{abs}(t_i)}{10^k} \tag{16}$$

The case where k is small must be considered, since points on the emitters might lie on or near the reference plane.

The phase distances from Eq. (14) depend critically on the physical location of the discretized emitter points. In the context of pointing a large laser array at a small, distant target, the optical axes of the emitters must be controllable. One method of adjusting an emitter optical axis would be to rotate the emitter element as a unit, i.e., the frame connecting the optical element and the fiber tip would move cohesively. In such a scenario, the position of discretized points on emitter surfaces would change relative to the reference plane. A more manageable approach might be to maintain the physical orientation (optical axis) of each emitter along a 'target vector' from the center of the array to the center of the target. Then, make small adjustments to the optical axis of each emitter by moving the fiber tip behind the optical element. One benefit of such an approach is that the exit phase across an emitter surface is constant with respect to the phase reference plane. Any electro-optic control of phase within the aperture of an emitter may be difficult to implement, so the model should not rely on such mechanisms.

2.2. Verification and Validation of the Near-Field Model

In order to check the model operation, several simulations are presented. The simulations all use an array of 7 emitters in a close-packed arrangement. The lens elements are 0.5 m in diameter, with the central emitter centered at the origin. The target surface is a plane that is 10 km directly in front of the array. First, in Fig. 4, a simulation was run with all optical axes pointing directly ahead. All of the emitter phases are 0 at the exit apertures, which are all aligned with the *x*-*y* plane. Energy from the individual array elements impinges on the target surface, with the pattern shown in Fig. 4. Results from two additional simulations are shown in Fig. 5. For these simulations, the optical axes of the emitters are all pointing directly at the center of the target plane. Results on the left of Fig. 5 are returned when no phase adjustment is applied. The pattern results from incoherent combination of the 7 beams, and there is no cohesive amplification in the central lobe. Results on the right of Fig. 5 are returned when the phases of each emitter are adjusted to be the same on the phase reference plane. When the phases are aligned, the results produce an amplified peak at the center of the target, where constructive phase interference occurs. The simulation results are in general agreement with what one would expect to see.

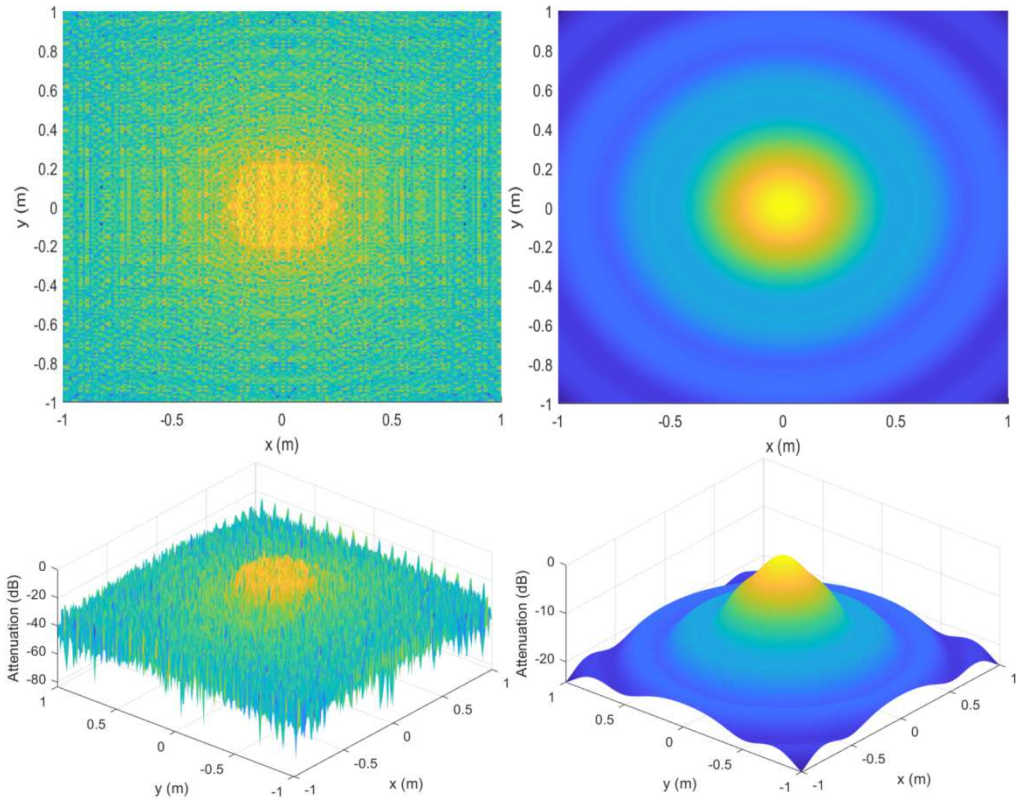

Figure 5. Pattern of light intensity on an orthogonal target plane 10 km from the source, which is the 7-element array depicted in Fig. 4. **Left**: The optical axes of all emitters are pointed at the center of the target plane. The phase of each emitter is set to zero at the exit aperture of every emitter, so the pattern in the target plane represents an incoherent combination of the 7 beams. **Right**: The optical axes of 7 emitters are pointed at the center of the target plane. The phase of each emitter is adjusted at the exit aperture to be in phase at the target surface, so the pattern in the center represents a coherent combination of 7 beams.

2.3. Incorporating Optical Axis and Phase Misalignments

In an operational system, the optical axes will be adjusted to point at the center of the target. The target will be accelerated by the directed-energy beam, and move away from the array. In this scenario, the optical axis of the center emitter will not change, but every other optical axis will have to be adjusted slightly as the distance to the target increases. Since the optical axes will be adjustable, there will always be a potential for both fixed and transient pointing errors. Additionally, as the optical axes are moved, the ray paths from the emitters to the phase reference plane will vary,

necessitating a phase control scheme. Phase adjustment will also be plagued with misalignment. The model described in Eq. (2) is general enough to incorporate fixed and time-varying optical axis and phase misalignments. Results of a simulation with errors in the optical axes of each emitter are shown in Fig. 6. The coherent combination of energy from the array is weakened, leading to a poorly formed beam. Note also that the axis of the combined beam is no longer pointing at the center of the target.

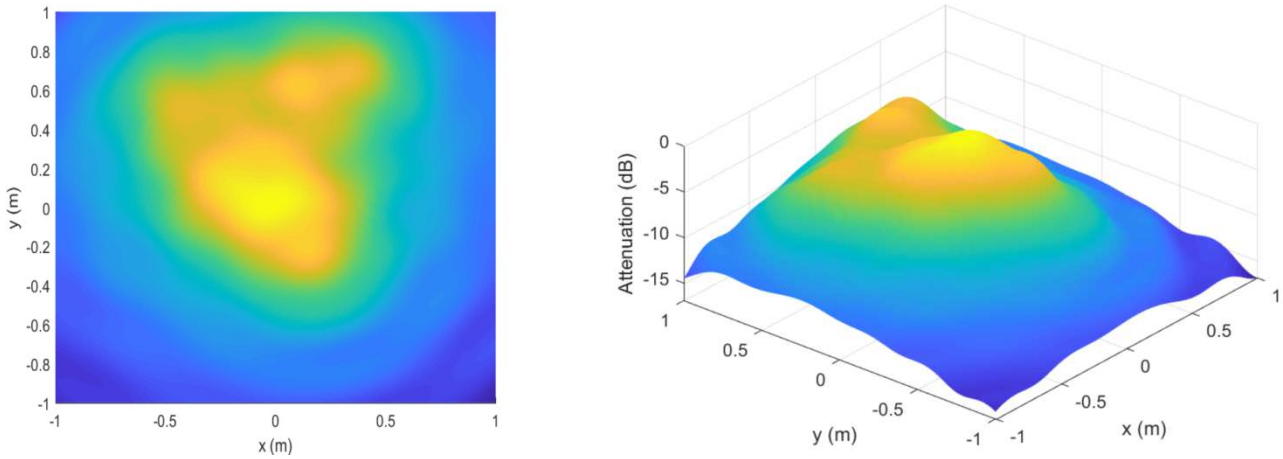

Figure 6. Pattern of light intensity on an orthogonal target plane 10 km from the source, which is the 7-element array depicted in Fig. 4. The optical axes of each emitter has been perturbed, so that they do not all point directly at the center of the target. Coherence of the beam is weakened, and the beam axis no longer points to the center of the target.

3. CONCLUSIONS

3.1. Progress to Date

Wafer-scale spacecraft are envisioned to begin interstellar missions in Earth orbit, deployed from a larger vessel. The spacecraft is accelerated to relativistic speeds (>0.1 *c*) by a directed-energy beam that delivers photon pressure to the spacecraft's reflective sail. The directed-energy beam is generated by a large array of phase-locked lasers. In order to investigate sail design and other mission parameters, an accurate model of the beam produced by such an array is required. Since the array is large, the initial distance to the spacecraft will not be supported by a far-field intensity model. This paper described a near-field optical model for an array of coherently combined laser emitters. The model is based on the sum of complex phases from all array elements as the phases are delivered to a target surface. First-order checks of the model using simulations indicate output characteristics that are consistent with the expected physics. The model can incorporate optical axis and phase misalignments, and additional simulations demonstrate the beam degradation resulting from such errors.

ACKNOWLEDGEMENTS

We gratefully acknowledge funding from the NASA California Space Grant NASA NNX10AT93H in support of this research. We also gratefully acknowledge funding from the NASA Innovative Advanced Concepts grant NNH15ZOA001N in support of this research.

REFERENCES

[1] Marx, G., "Interstellar vehicle propelled by terrestrial laser beam," *Nature* 211, 22-23 (1966).

[2] Redding, J. L. "Interstellar vehicle propelled by terrestrial laser beam," *Nature* 213, 588-589 (1967).

[3] Matloff, G.L. and Mallove, E., "Solar sail starships: the clipper ships of the galaxy," *Journal of the British Interplanetary Society*, v. 34, pp.371-380 (1981).

[4] Forward, R. L., “Roundtrip interstellar travel using laser-pushed lightsails,” *Journal of Spacecraft and Rockets*, v. 21, 187-195 (1984).

[5] Beals, K. A., Beaulieu, M., Dembia, F. J., Kerstiens, J., Kramer, D. L., West, J. R., and Zito, J. A., “Project Longshot: An Unmanned Probe to Alpha Centauri,” US Naval Academy, NASA-CR-184718, (1988).

[6] Crawford, I.A., “Interstellar travel: a review for astronomers,” *Quarterly Journal of the Royal Astronomical Society*, v. 31, pp.377-400 (1990).

[7] Simmons, J.F.L. and McInnes, C.R., “Was Marx right? or How efficient are laser driven interstellar spacecraft?,” *American Journal of Physics*, 61(3), pp.205-207 (1993).

[8] Kare, J.T. “High acceleration micro-scale laser sails for interstellar propulsion,” *Final Report, NIAC Research Grant*, pp.07600-070 (2002).

[9] Taylor, T., Anding, R.C., Halford, D. and Matloff, G.L. “Space based energy beaming requirements for interstellar laser sailing,” *Beamed Energy Propulsion: First International Symposium on Beamed Energy Propulsion*, 664(1), pp. 369-381 (2003).

[10] Long, K.F., *Deep Space Propulsion: A Roadmap to Interstellar Flight*. Springer Science & Business Media (2011).

[11] Bae, Y. K., “Prospective of photon propulsion for interstellar flight,” *Physics Procedia* 38, 253-279 (2012).

[12] Bible, J., Bublitz, J., Johansson, I.E., Hughes, G.B., and Lubin, P. “Relativistic Propulsion Using Directed Energy,” *Nanophotonics and Macrophotonics for Space Environments VII*, edited by Edward W. Taylor, David A. Cardimona, Proc. of SPIE, Vol. 8876, 887605 (2013).

[13] Lubin, P., Hughes, G.B., Bible, J. and Johansson, I. “Directed Energy for Planetary Defense and Exploration: Applications to Relativistic Propulsion and Interstellar Communications,” *Journal of the British Interplanetary Society*, vol. 68, no. 5/6, pp. 172-182 (2015).

[14] Lubin, P. “A Roadmap to Interstellar Flight,” *Journal of the British Interplanetary Society*, Vol. 69, no. 6/7, pp.40-72 (2016).

[15] Zhang, Q., Walsh, K.J., Melis, C., Hughes, G.B., and Lubin, P. “Orbital simulations of laser-propelled spacecraft,”*Nanophotonics and Macrophotonics for Space Environments IX*, edited by Edward W. Taylor, David A. Cardimona, Proc. of SPIE Vol. 9616 (2015).

[16] Brashears, T., Lubin, P., Hughes, G.B., McDonough, K., Arias, S., Lang, A., Motta, C., Meinhold, P., Batliner, P., Griswold, J., Zhang, Q., Alnawakhtha, Y., Prater, K., Madajian, J., Sturman, O., Gergieva, J., Gilkes, A., and Silverstein, B. “Directed Energy Interstellar Propulsion of WaferSats,”*Nanophotonics and Macrophotonics for Space Environments IX*, edited by Edward W. Taylor, David A. Cardimona, Proc. of SPIE Vol. 9616 (2015).

[17] Brashears, T., Lubin, P., Rupert, N., Stanton, E., Mehta, A., Knowles, P., and Hughes, G.B. “Building the future of wafersat spacecraft for relativistic spacecraft,” *Planetary Defense and Space Environment Applications*, edited by Gary B. Hughes, Proc. Of SPIE Vol. 9981, pp. 998103 (2016).

[18] Manchester, Z. and Loeb, A. “Stability of a Light Sail Riding on a Laser Beam,” *The Astrophysical Journal Letters*, Vol. 837, No. 2, p. L20 (2017).

[19] Srinivasan, P., Hughes, G.B., Lubin, P., Zhang, Q., Madajian, J., Brashears, T., Kulkarni, N., Cohen, A., and Griswold, J. “Stability of laser-propelled wafer satellites,” *Planetary Defense and Space Environment Applications*, edited by Gary B. Hughes, Proc. Of SPIE Vol. 9981, pp. 998104 (2016).

[20] Kare, J.T. “High acceleration micro-scale laser sails for interstellar propulsion,” *Final Report, NIAC Research Grant*, pp.07600-070 (2002).

[21] Landis, G.A. “Advanced Solar-and Laser-pushed Lightsail Concepts,” NASA Innovative Advanced Concepts Final Report (1999).

[22] Hughes, G.B., Lubin, P., Griswold, J., Bozinni, D., O’Neill, H., Meinhold, P., Suen, J., Bible, J., Riley, J., Johansson, I., Pryor, M. and Kangas, M. “Optical modeling for a laser phased-array directed energy system,” *Nanophotonics and Macrophotonics for Space Environments VIII*, edited by Edward W. Taylor, David A. Cardimona, Proc. of SPIE, Vol. 9226 (2014).

[23] Hughes, G.B. “Algorithms for sensor chip alignment to blind datums,” *Journal of Electronic Imaging*, 15(3), 033003 (2006).